Electronic Supplementary Information (ESI) for

Moisturized 2-dimensional halide perovskite generates a power density of 30 mW cm^{-3}

Chunqing Ma,[1‡] Yeon-Woo Choi,[1‡] Donghyeon Kang,[2‡] Bosung Kim,[3] Seung-Gu Choi,[4] Jin-Wook Lee,[4] Sang-Woo Kim,[3*] Nam-Gyu Park[1,5*]

[1]School of Chemical Engineering and Center for Antibonding Regulated Crystals, Sungkyunkwan University, Suwon 16419, Republic of Korea

[2]School of Advanced Materials Science and Engineering, Sungkyunkwan University, Suwon 16419, Republic of Korea

[3]Department of Materials Science and Engineering, Center for Human-oriented Triboelectric Energy Harvesting, Yonsei University, Seoul 03722, Republic of Korea

[4]Department of Nano Engineering and Department of Nano Science and Technology, SKKU Advanced Institute of Nanotechnology (SAINT), Sungkyunkwan University, Suwon 16419, R epublic of Korea

[5]SKKU Institute of Energy Science and Technology (SIEST), Sungkyunkwan University, Suwon 16419, Republic of Korea

‡ These authors contributed equally to the work

*Corresponding Authors: kimsw1@yonsei.ac.kr; npark@skku.edu

Supplementary materials include

Figures S1-S18,

Tables S1,

and References.

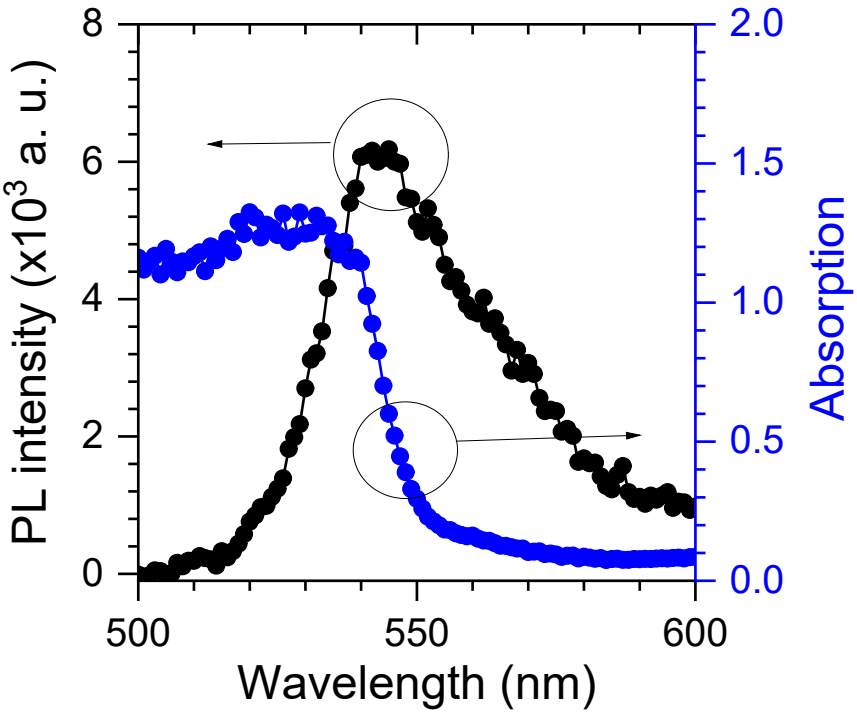

Fig. S1. Absorbance and steady-state PL of the 2D perovskite.

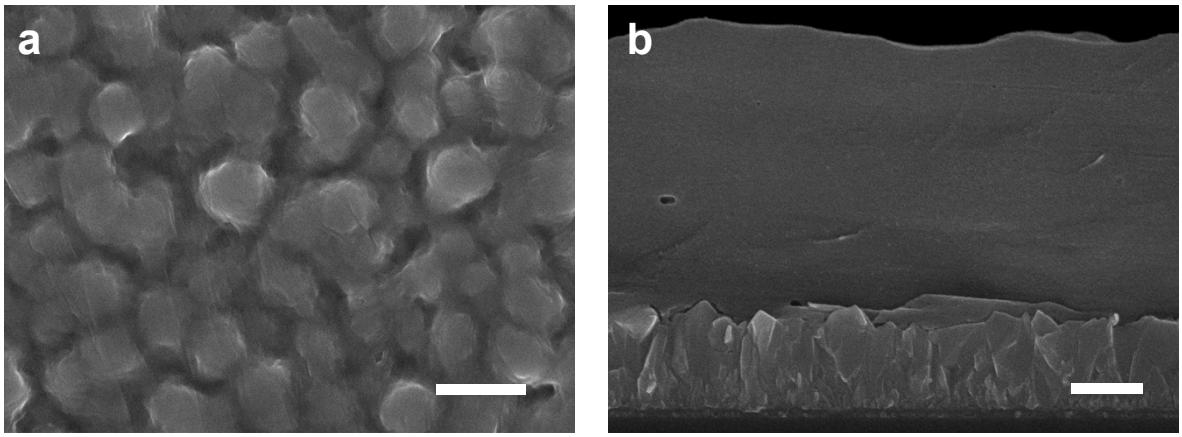

Fig. S2. (a) Surface and (b) cross-sectional SEM images of the 2D perovskite thin film. Scale bars are (a) 2 μm and (b) 500 nm.

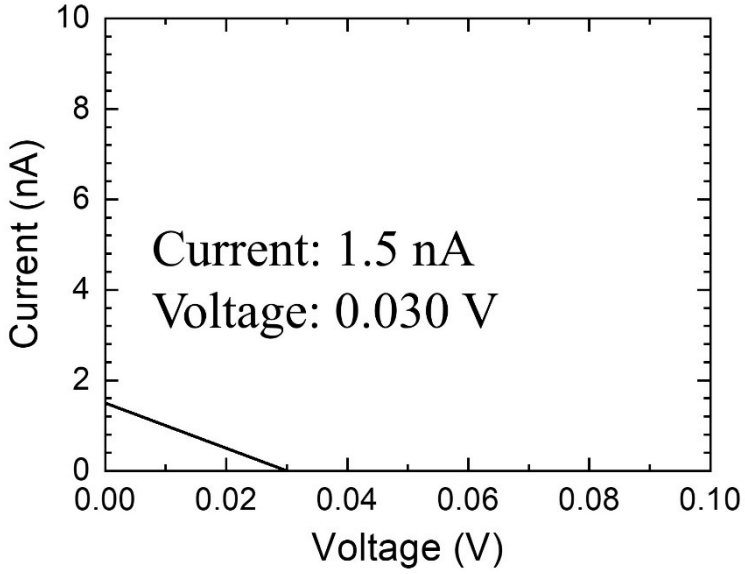

Fig. S3. Performance of the ionovoltaic device under 1-sun illumination.

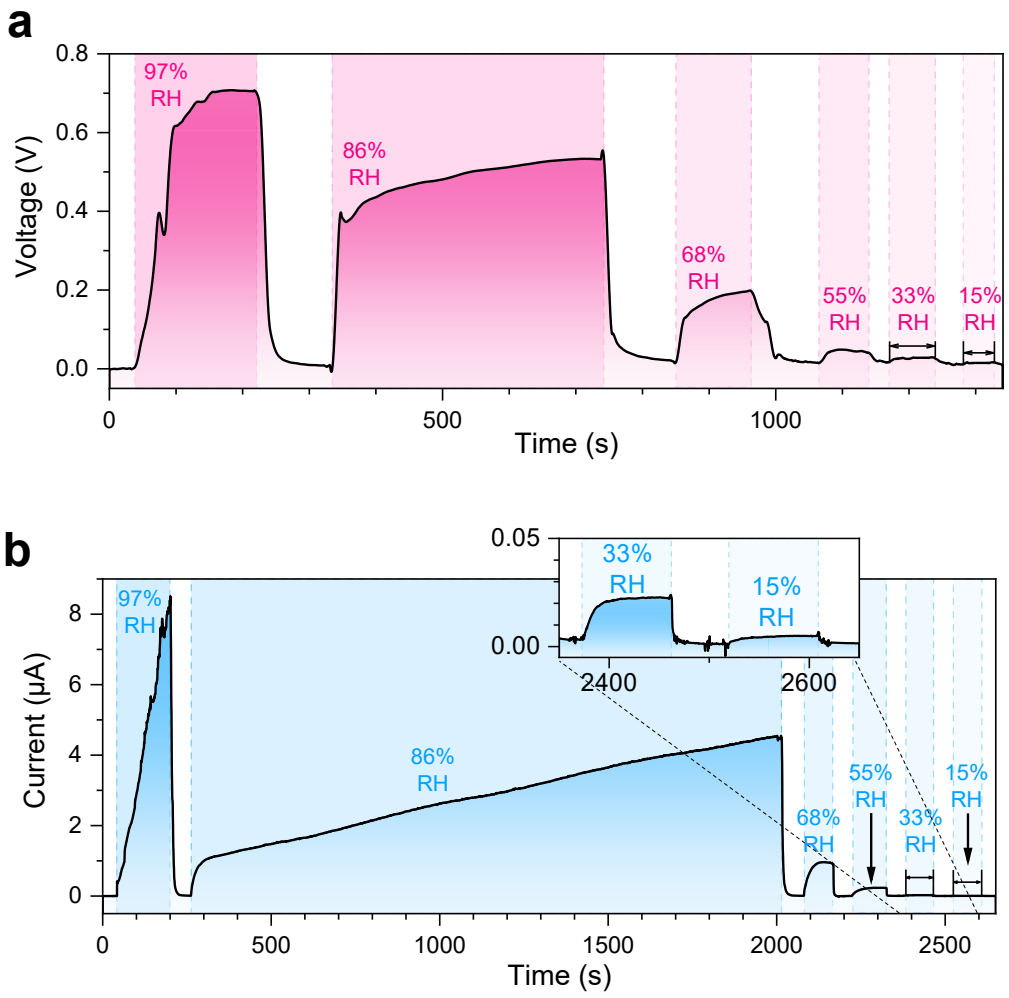

Fig. S4. (a) V-t and (b) I-t graph of the device under 15%, 33%, 55%, 68%, 86% and 97% RH exposure at 20 °C. Colored regions are humidity-exposed periods.

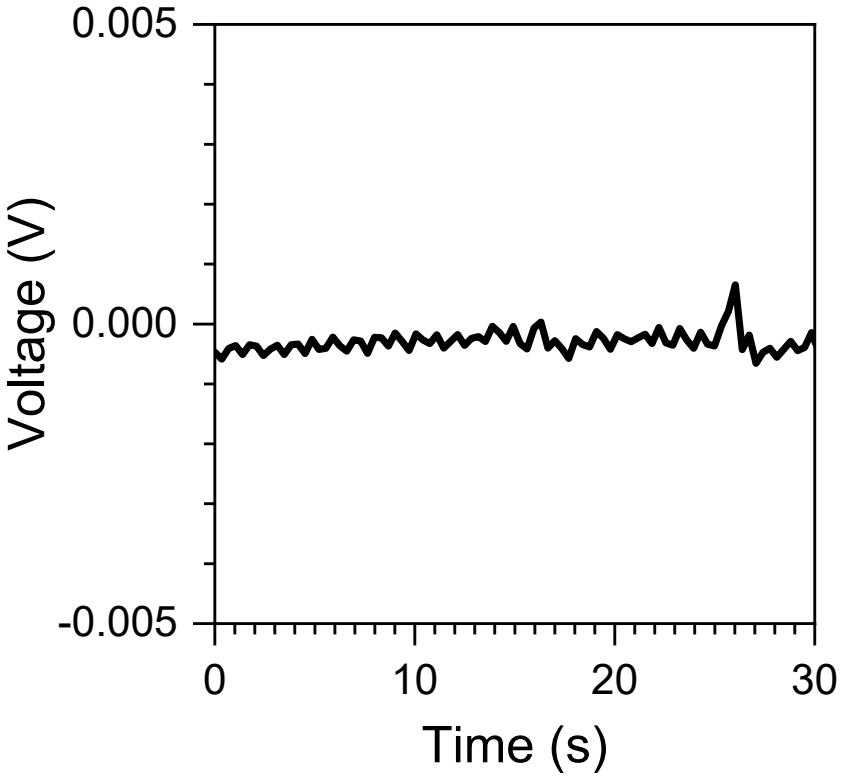

Fig. S5. V-t measurement result under 0.4% RH, 20 °C.

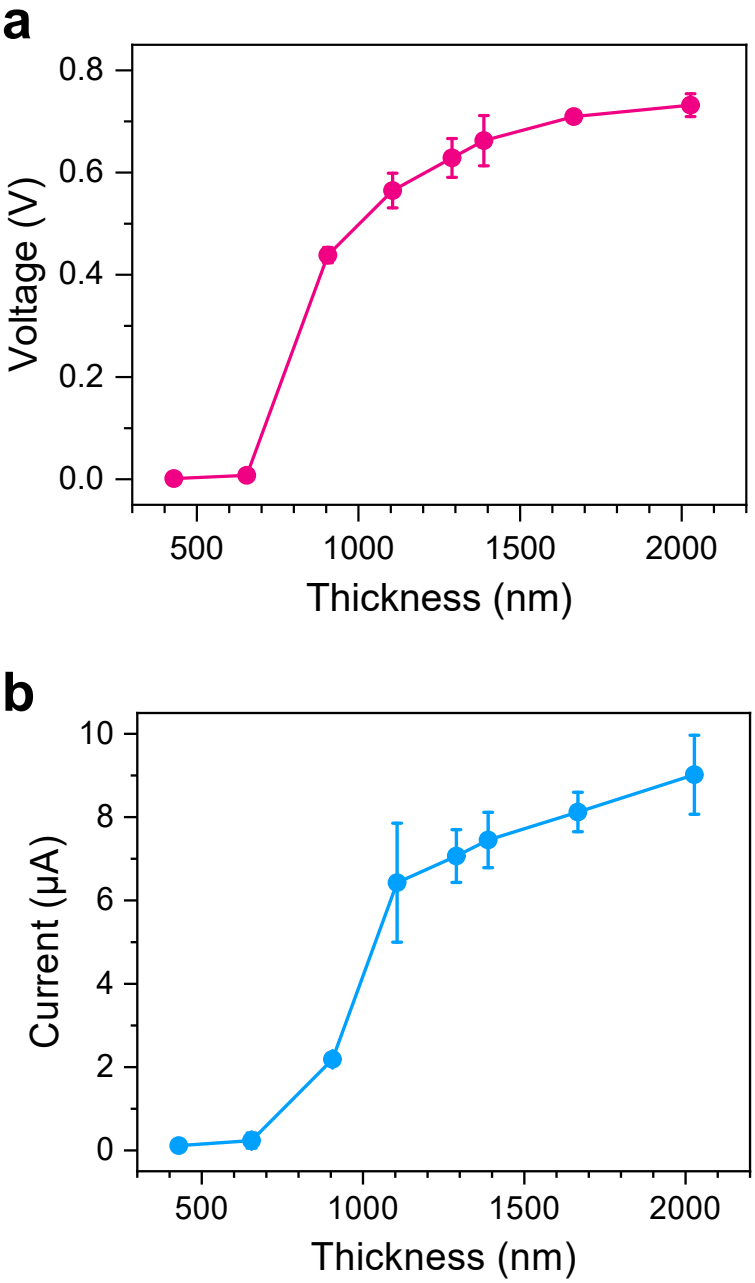

Fig. S6. (a) Voltage and (b) current performances from *V-t* and *I-t* measurements with different perovskite thicknesses. Devices were exposed to 97% RH at 20 °C.

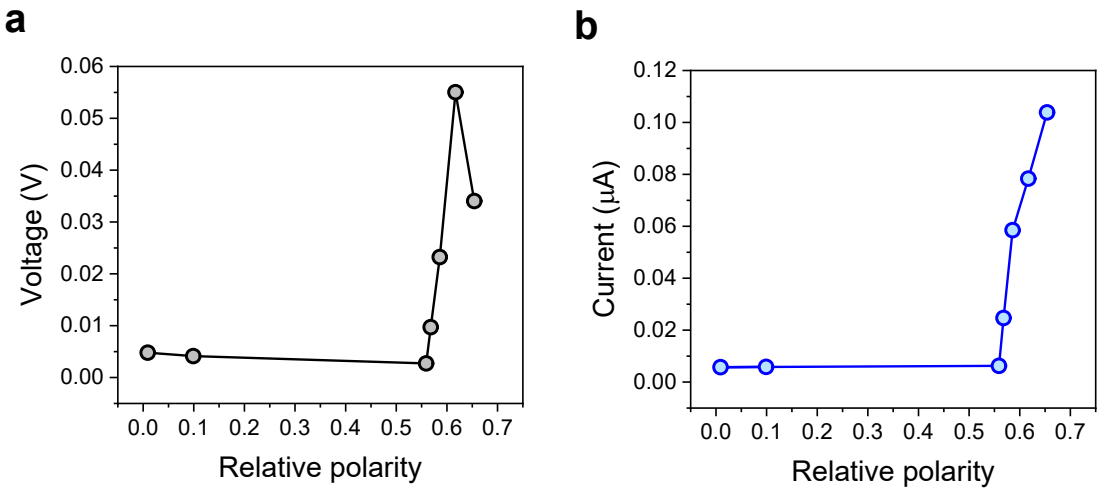

Fig. S7. Voltage and current performance obtained from V-t and I-t measurements by exposure to the vapor of alcohols with different alkyl chain lengths (ethanol, 1-propanol, 1-butanol, 1-pentanol and 1-hexanol), toluene and hexane at 20 °C. Relative polarity of solvents is ethanol (0.654), 1-propanol (0.617), 1-butanol (0.586), 1-pentanol (0.568), 1-hexanol (0.559), toluene (0.099) and hexane (0.009).

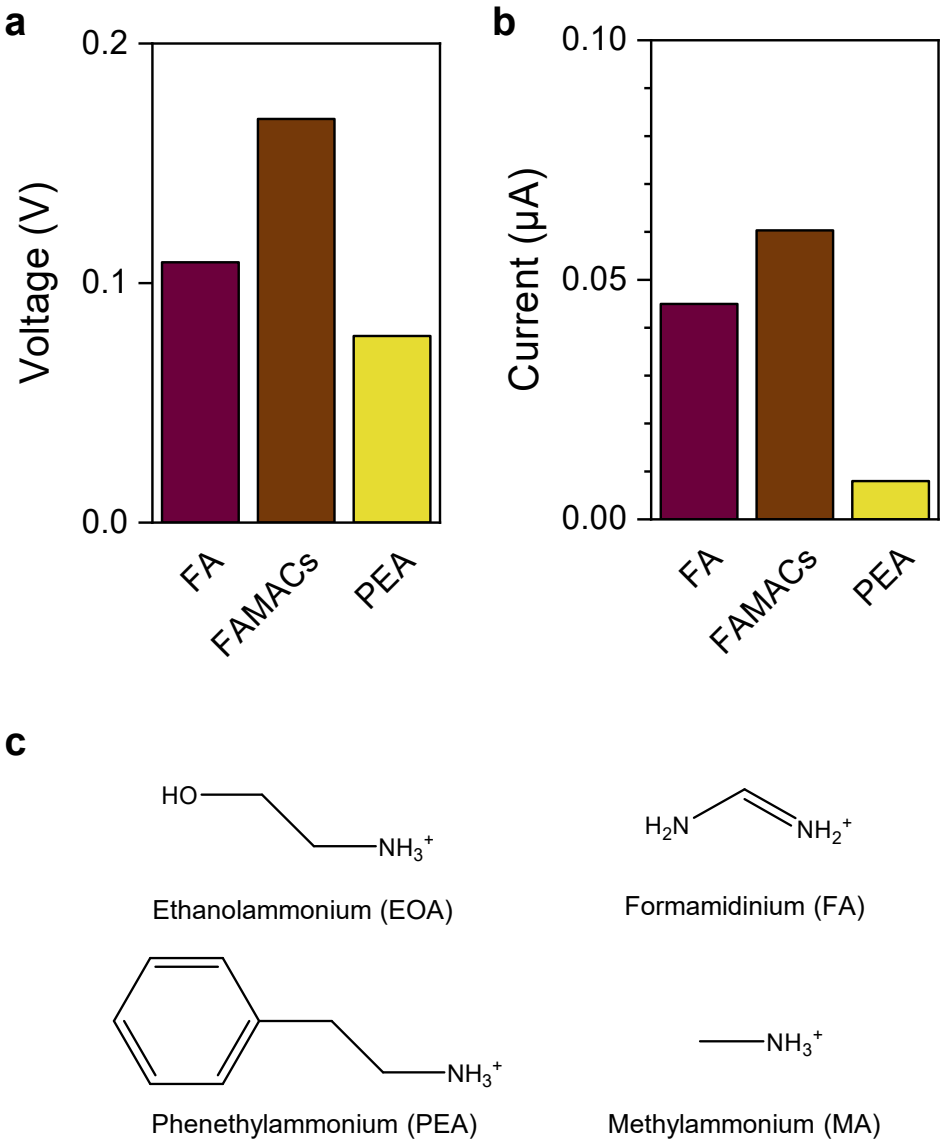

Fig. S8. (a) Voltage and (b) current performance from *V-t* and *I-t* measurements of devices with $FAPbI_3$, $FA_{1-x-y}MA_xCs_yPb(I_{3-z}Br_z)_3$ (FAMACs) 3D perovskite and PEA_2PbI_4 2D perovskite exposed to 97% RH at 20 °C. (c) Illustration of the organic cations. All perovskite films were deposited with the same coating condition as EOA_2PbI_4 device.

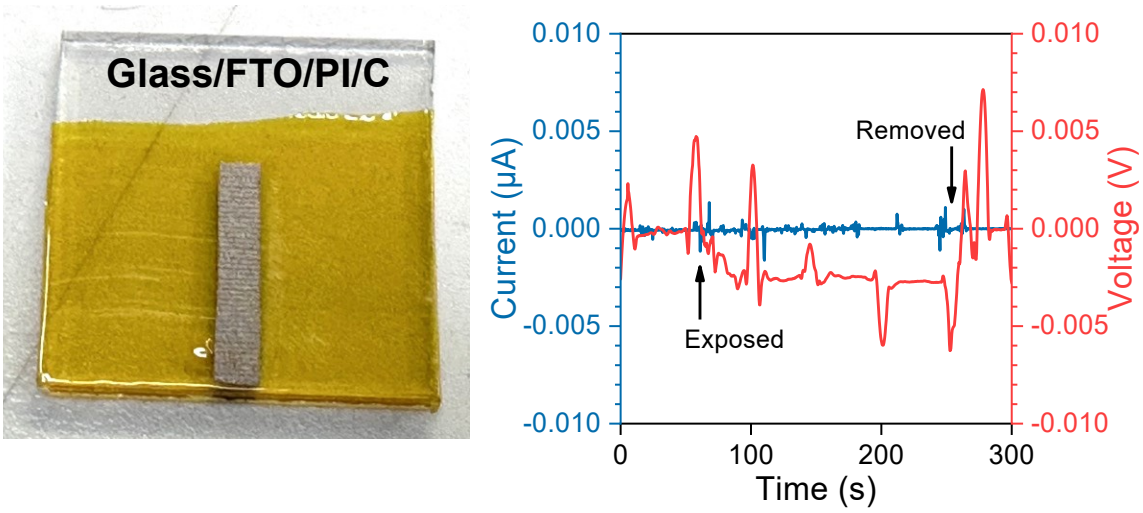

Fig. S9. I-t and V-t measurement results of device with a structure of carbon electrode/Poly imide (PI)/etched FTO/Glass under 97% RH at 20 ºC.

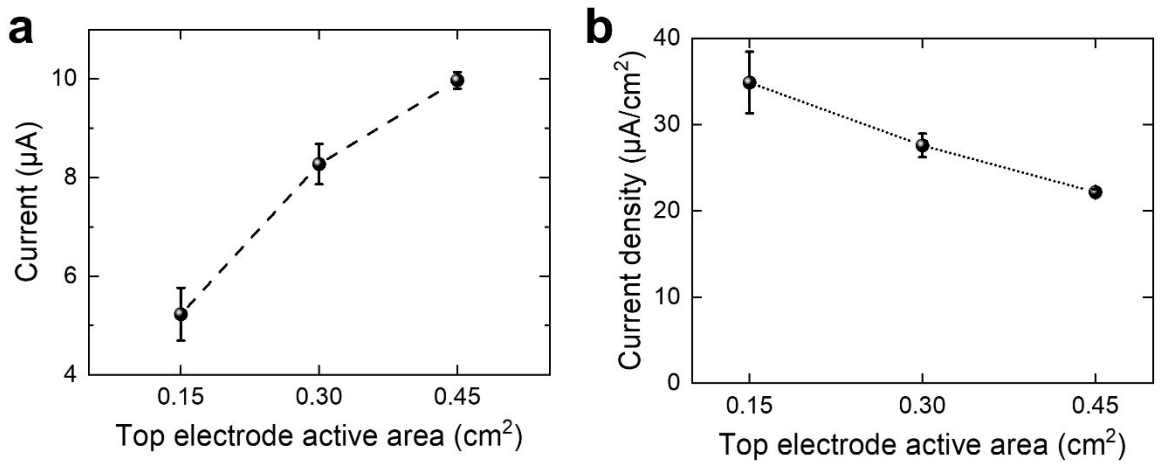

Fig. S10. (a) Current and (b) current density values from devices with different active area sizes (1.5×10 mm, 3×10 mm and 4.5×10 mm) under 97% RH at 20 °C.

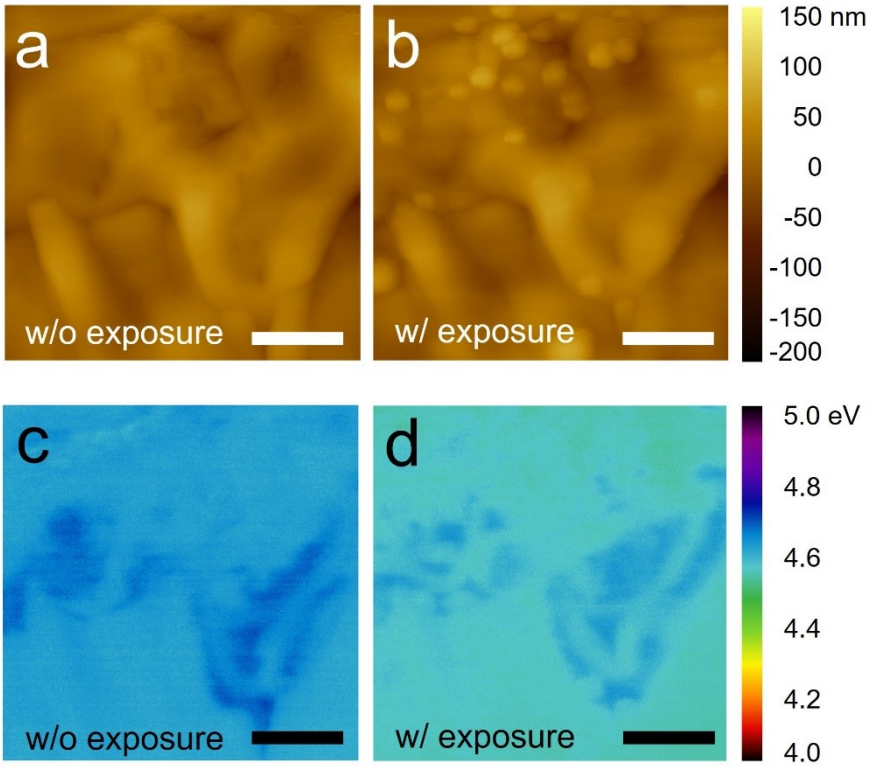

Figure S11. AFM topology images of perovskite before (a) and after (b) exposure to humid air (~55% RH, 25°C). KPFM images of perovskite before (c) and after (d) exposure to humid condition (~55% RH, 25°C). Scale bars indicate 500 nm.

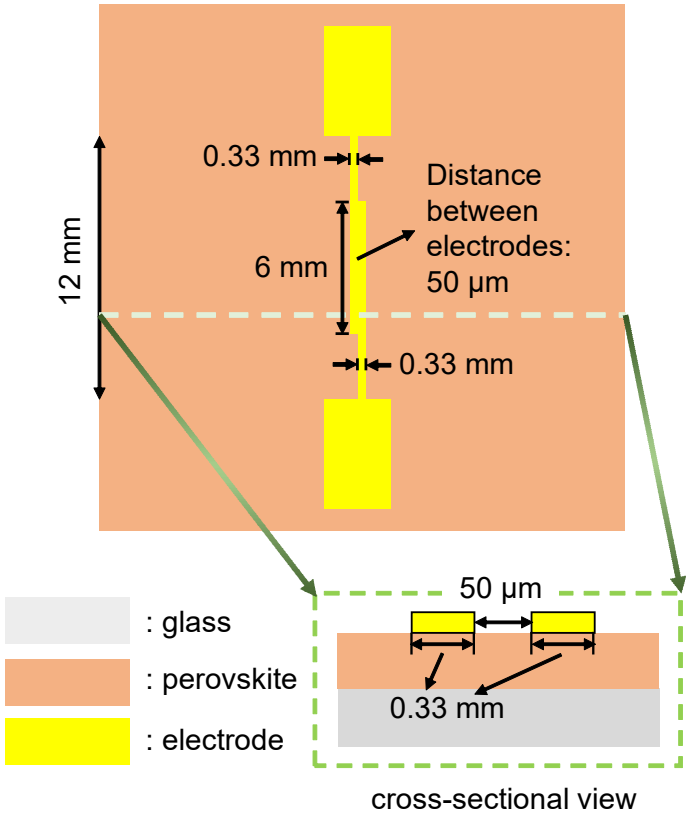

Fig. S12. Device structure for measuring surface ionovoltaic properties that were presented in Fig. 3(g).

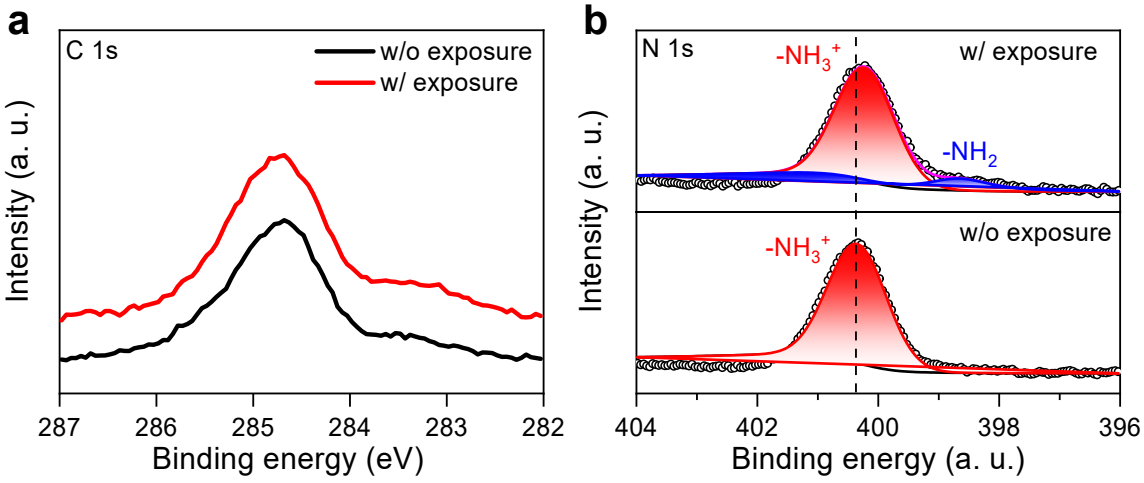

Fig. S13. (a) C 1s and (b) N 1s XPS data for perovskite films without and with exposure under 86% RH at 20 °C.

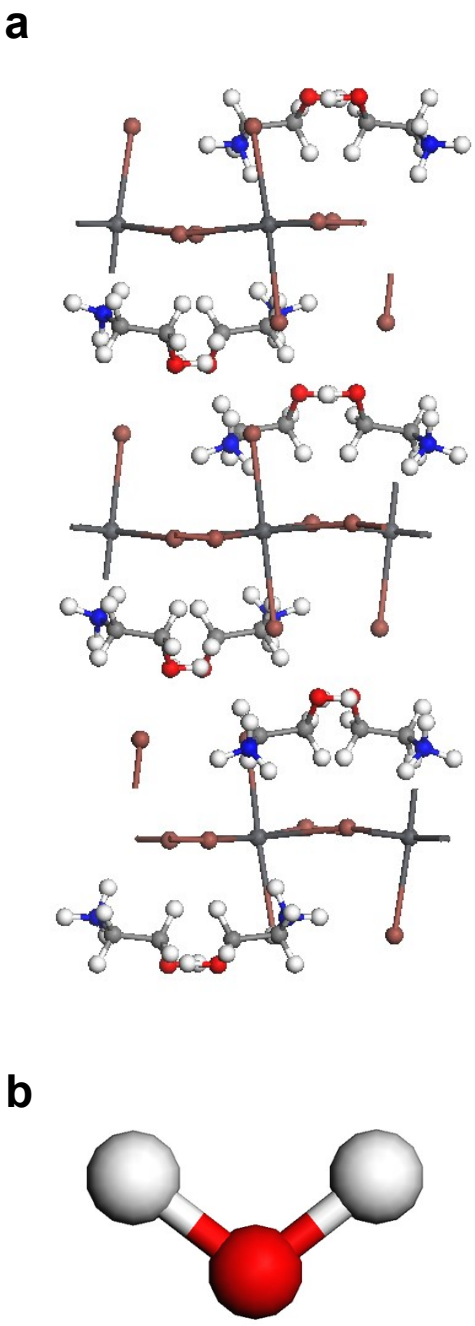

Fig. S14. Optimized structure of (a) EOA_2PbI_4 and (b) H_2O.

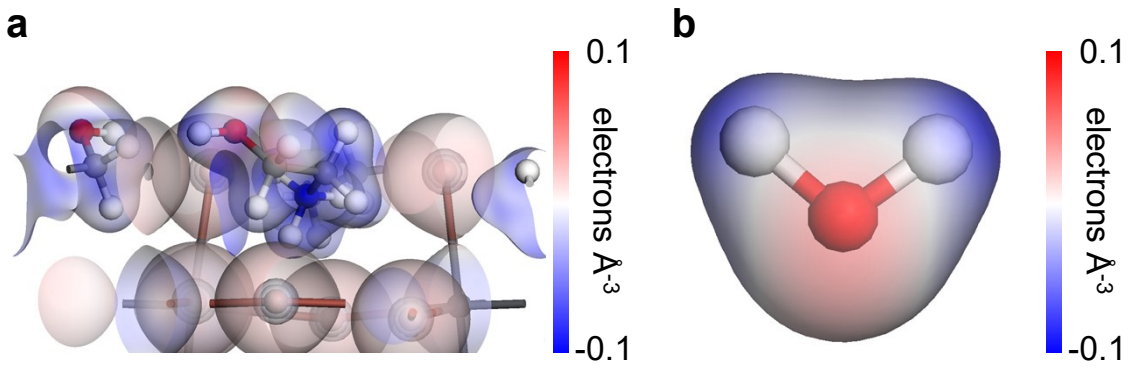

Fig. S15. The local potential in (a) EOA_2PbI_4 and (b) H_2O analyzed using electron density difference (EDD).

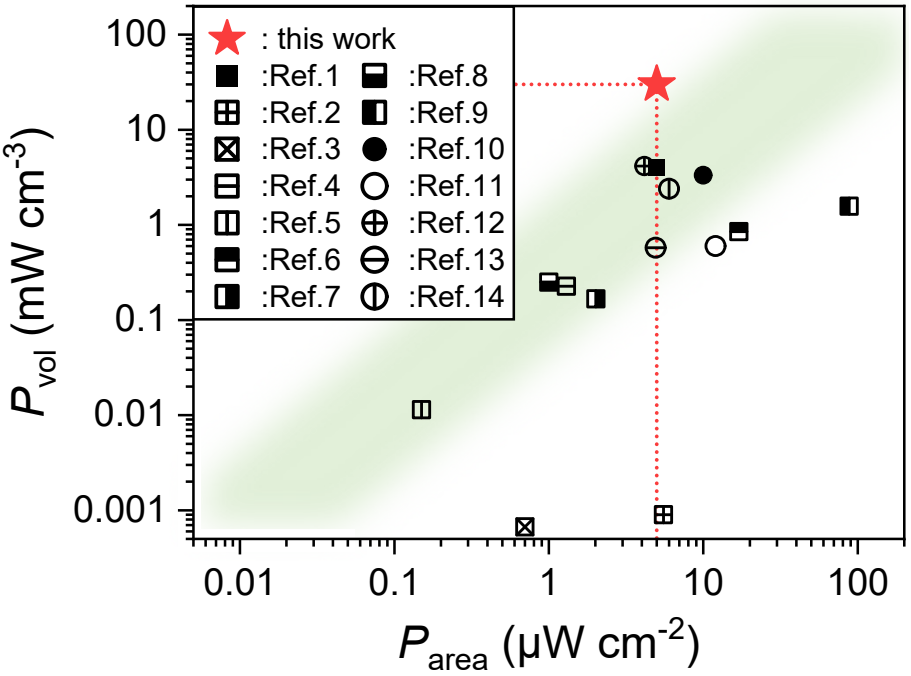

Fig. S16. Volumetric (P_{vol}) and areal power densities (P_{area}) of the current perovskite ionovoltaics (star) and the previously reported data published elsewhere [1-14].

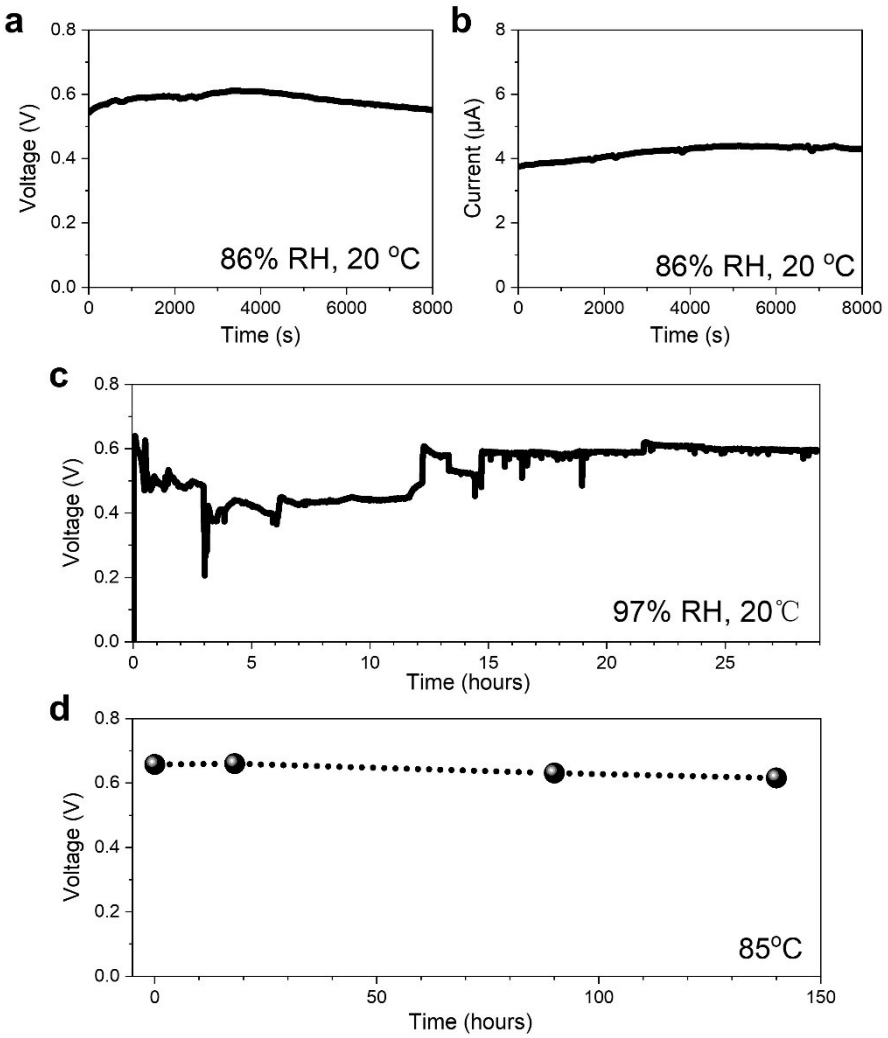

Fig. S17. (a) *V-t* and (b) *I-t* measured for 8000 seconds under 86% RH at 20 °C, (c) *V-t* measured for 29 hours under 97% RH at 20 °C, (d) thermal stability of the device stored under 85°C.

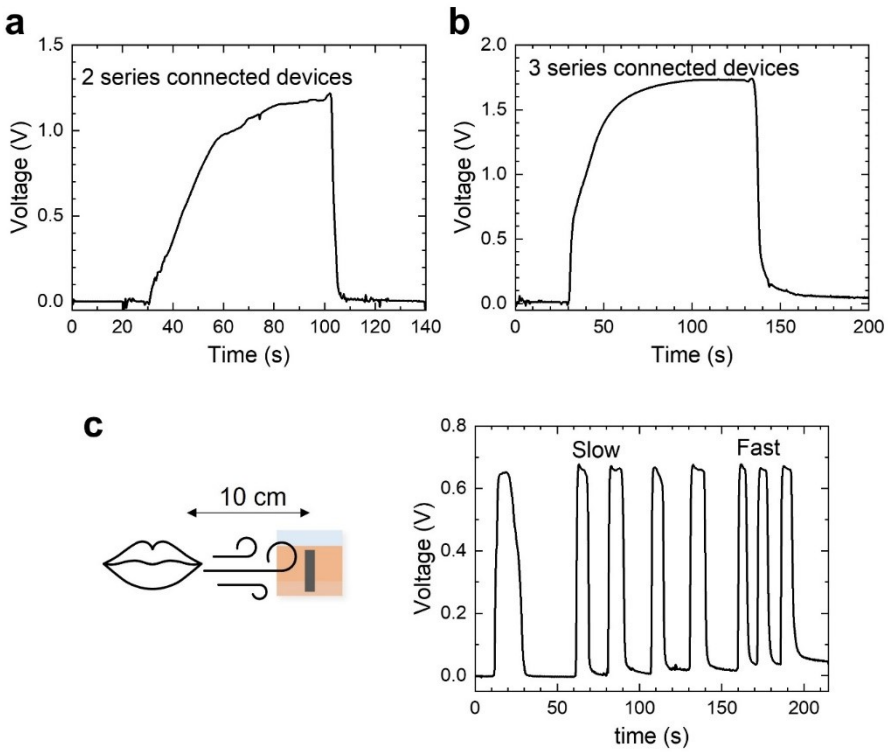

Fig. S18. Voltage output of the series connected devices with (a) 2 and (b) 3 devices. (c) Application of ionovoltaic devices for respiration sensors.

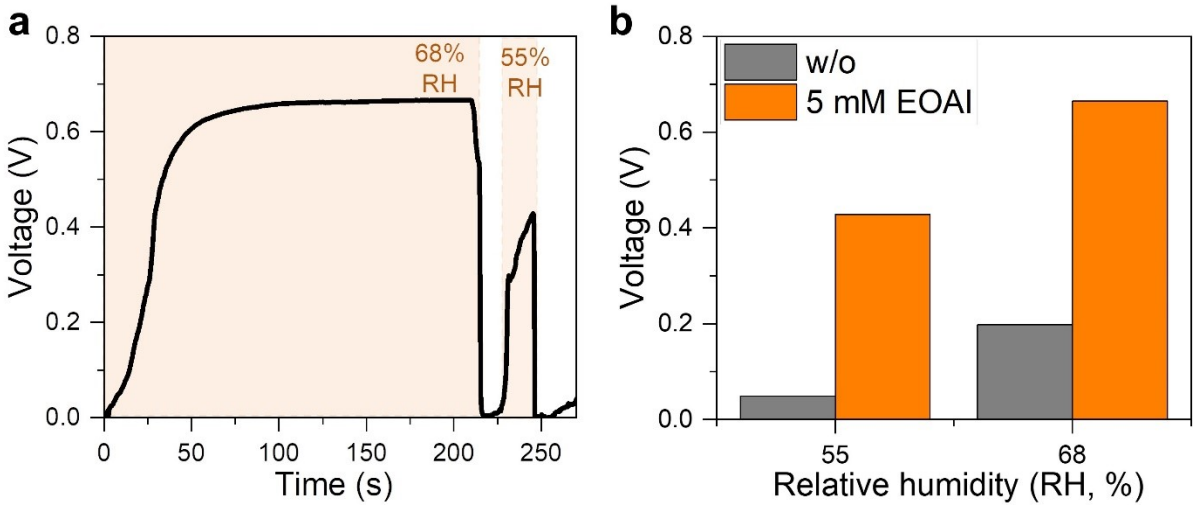

Fig. S19. Voltage output of the modified perovskite ionovoltaic device with 5 mM EOAI under 55 and 68% RH.

Table S1. Areal and volumetric power densities of ionovoltaics with various active materials.

Materials	RH	Areal Power density ($\mu W\ cm^{-2}$)	Active layer thickness (μm)	Voltage performance (V)	Volumetric Power density ($mW\ cm^{-3}$)	Ref.
2D Perovskite	**97%**	**4.99**	**1.67**	**0.7**	**30**	**this work**
protein nanowires	50%	5	7	0.5	4	1
polyelectrolyte bilayers	85% (25%)	5.52 (0.076)	100	1.38 (0.95)	0.552* (9×10^{-4})	2
LiCl + Carbon black + cellulon	55~60 %	0.7	2000	0.78	6.7×10^{-4}	3
CNT/AAO	93%	1.3	47	1.1	0.227	4
electrolyte-loaded nanofiber	95%	0.15	132	0.7	0.0114	5
PSSA membrane	80%	17	200	0.8	0.85*	6
Graphene oxide	85%	2.02	120	0.45	0.168*	7
Microbial biofilms	50%	1.0	40	0.45	0.25*	8
PSSA/Rose Bengal	50%	88	560	0.92	1.571*	9
Silicon Nanowire fibers	63%	10	30	0.55	3.33*	10
Sodium alginate + SiO_2 + rGO	100%	12	200	0.5	0.6*	11
TiO_2 nanowire	85%	4.16	10	0.5	4.16*	12
Cellulose membrane	82%	4.92	85	0.83	0.576*	13

silicon nanowire arrays	45%	6	25	0.4	2.4*	14
Calcinated ZIF-8/GO + ILs	93%	109.2	-	0.3	**	15

* Marked power densities were calculated based on the thickness of active layers.
** The calculation was excluded because of the complicated system by the existence of multiple layers that could be involved in power density measurement.

References

1. X. Liu, H. Gao, J. E. Ward, X. Liu, B. Yin, T. Fu, J. Chen, D. R. Lovley and J. Yao, *Nature*, 2020, **578**, 550-554.
2. H. Wang, Y. Sun, T. He, Y. Huang, H. Cheng, C. Li, D. Xie, P. Yang, Y. Zhang and L. Qu, *Nat. Nanotechnol.*, 2021, **16**, 811–819.
3. J. Tan, S. Fang, Z. Zhang, J. Yin, L. Li, X. Wang and W. Guo, *Nat. Commun.*, 2022, **13**, 3643.
4. Y. Zhang, T. Yang, K. Shang, F. Guo, Y. Shang, S. Chang, L. Cui, X. Lu, Z. Jiang, J. Zhou, C. Fu and Q.-C. He, *Nat Commun.*, 2022, **13**, 3484.
5. Z. Sun, X. Wen, L. Wang, J. Yu and X. Qin, *Energy Environ. Sci.*, 2022, **15**, 4584.
6. T. Xu, X. Ding, Y. Huang, C. Shao, L. Song, X. Gao, Z. Zhanga and L. Qu, *Energy Environ. Sci*., 2019, **12**, 97.
7. H. Cheng, Y. Huang, F. Zhao, C. Yang, P. Zhang, L. Jiang, G. Shi and L. Qu, *Energy Environ. Sci.*, 2018, **11**, 2839.
8. X. Liu, T. Ueki, H. Gao, T. L. Woodard, K. P. Nevin, T. Fu, S. Fu, L. Sun, D. R. Lovley and J. Yao, *Nat Commun.*, 2022, **13**, 4369.
9. J. Bai, Y. Huang, H. Wang, T. Guang, Q. Liao, H. Cheng, S. Deng, Q. Li, Z. Shuai and L. Qu, *Adv. Mater.*, 2022, **34**, 2103897.
10. B. Shao, Z. Song, X. Chen, Y. Wu, Y. Li, C. Song, F. Yang, T. Song, Y. Wang, S.-T. Lee and B. Sun, *ACS Nano*, 2021, **15**, 7472-7481.
11. H. Wang, T. He, X. Hao, Y. Huang, H. Yao, F. Liu, H. Cheng and L. Qu, *Nature Commun.*, 2022, **13**, 2524.
12. D. Shen, M. Xiao, G. Zou, L. Liu, W. W. Duley and Y. N. Zhou, *Adv. Mater.*, 2018, **30**, 1705925.
13. S. Lee, J. Eun and S. Jeon, *Nano Energy*, 2020, **68**, 104364.
14. Y. Qin, Y. Wang, X. Sun, Y. Li, H. Xu, Y. Tan, Y. Li, T. Song and B. Sun, *Angew. Chem. Int. Ed.*, 2020, **59**, 10619-10625.
15. D. Lv, S. Zheng, C. Cao, K. Li, L. Ai, X. Li, Z. Yang, Z. Xu and X. Yao, *Energy Environ. Sci.*, 2022, **15**, 2601-2609.